Change in Marine Environment after Artificial Reef Deployment in the South Sea of Korea

Kim, Dong-Sun
Research Center for Ocean Industrial Development (RCOID), Pukyong National University

Shimasaki, Yohei
Laboratory of Marin Environmental Science, Division of Animal & Marine Bioresource Sciences, Department of Bioresource Sciences, Faculty of Agriculture, Kyushu University

https://doi.org/10.5109/27373

出版情報：九州大学大学院農学研究院紀要. 58 (2), pp.403-415, 2013-09. Faculty of Agriculture, Kyushu University
バージョン：
権利関係：

J. Fac. Agr., Kyushu Univ., **58** (2), 403–415 (2013)

Change in Marine Environment after Artificial Reef Deployment in the South Sea of Korea

Dong–Sun KIM[1] and Yohei SHIMASAKI*

Laboratory of Marin Environmental Science, Division of Animal & Marine Bioresource Sciences,
Department of Bioresource Sciences, Faculty of Agriculture,
Kyushu University, Fukuoka 812–8581, Japan
(*Received April 26, 2013 and accepted May 9, 2013*)

In order to study the change of marine environment after artificial reef deployment in the South Sea of Korea, water temperature, currents and nutrients distributions were investigated during the strongly stratified summer season. Before the deployment of artificial reef, the maximum thermocline of water column (MTWC) formed at depths of 30~40 m in almost all of the studied area. However, after the deployment of the artificial reef, depending on tide time, variations in MTWC were observed about 10~17 m shallower in areas within 1 km in radius of the artificial reef due to uplifting of isotherms. In waters surrounding the artificial reef, vertical currents alternate between local downwelling flow (LDF) and local upwelling flow (LUF), and this type of phenomenon is dependent on tide time and takes on various patterns of spatial distribution. In addition, the degree of vertical mixing, which can be deduced from areas with strong current shears, especially in the surrounding area of the artificial reef from which the LUF originates, was found to be distributed in a similar manner. Although there are tide time–dependent differences in the Richardson number (Ri), in depths of 30~40 m or deeper, where the Ri is less than 0.25, the water column was destabilized by vertical mixing. In addition, differences in nutrient distribution were noted before and after the artificial reef deployment. Highly stratified nutrients rose to the upper layer after passing the artificial reef, and the accumulation of nutrients can be attributed to the LUF developingat the artificial reef. Thus, in periods of strong stratification during the summer, the upward movement of nutrients from the aphotic to the euphotic layer increases the primary production levels, triggering the formation of a marine food chain in those areas.

Key words: artificial reef, current shear, local downwelling flow (LDU), local upwelling flow (LUP), Richardson number

INTRODUCTION

Throughout the world, upwelling fishing grounds are located at the coastal regions of California, Peru, Northwest Africa, Benguela, and Somalia. In such regions, as a result of sudden increases in primary production levels (Barber and Smith, 1981), favorable fishing grounds form as many schools of fish are attracted to the regions (Boje and Tomczak, 1978; Cushing, 1971). Only 0.1% of the total ocean consists of upwelling fishing grounds, such areas are responsible for nearly 50% of the total fisheries production (Cushing, 1969; Ryther, 1969).

Currently, in some deep sea areas of coastal zones, there are efforts to increase the primary production levels of the photic layers through artificial upwelling of nutrients, which have accumulated in the bottom waters over the summer season, induced via structural deployments. In Japan, for example, artificial upwelling structures (10×10×45 m) deployed in the Uwajima coastline of the Bungo Strait resulted in increased tidal current velocity. Also the concentration of chlorophyll–a and number of zooplankton were increased 2–3 times near the surface. Fish population showed to have increased after three years of deployment (Yanagi and Nakajima, 1991). In addition, in the Kitamatsura coast of Nagasaki, the levels of primary production showed to have increased after deploying artificial upwelling structures (14×40×120 m) (Suzuki, 2002).

From a biological standpoint, the formation of the coastal front leads to the high primary productivity of the region, with abundant zooplankton (Chung and Yang, 1991; Kim *et al*., 1993; Park and Choi, 1997; Simpson *et al*., 1982). The area serves as good spawning and nursery grounds for fish species, such as anchovies and mackerels, as its temperatures are higher than of the neighboring East and West Seas, and have been shown to be economically important fish farming areas (Kim, 1992; OECD, 1997).

Recently, however, the fishery environment of the Korean coast has been worsening at increasing rates as a result of urbanization and industrialization, in addition to industrial and water waste from the land, and consequent consistent marine environment pollution (FAO, 1998). In addition, the Three Gorges Dam, located upstream of the Yangtze River, contributes to the decrease in the nutrient inflow, as well as to changes in water temperatures and salinity levels, to the western and southern coast of Korea and is expected to affect the area's fishery environment (Lee and Kim, 2007). Further, the designation of the Exclusive Economic Zones (EEZ) from surrounding nations, such as Japan and China, has led to a decrease in available fishing grounds and the consequent reduction in fisheries resources. Such coastal environmental changes and

[1] Research Center for Ocean Industrial Development (RCOID), Pukyong National University, Busan 608–737, Republic of Korea
* Corresponding author (E–mail: simasaki@agr.kyushu–u.ac.jp)

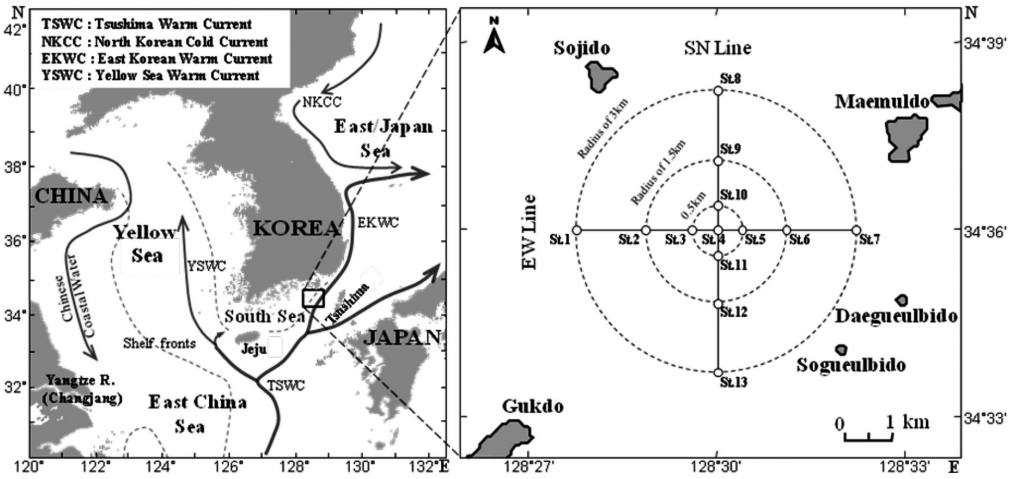

Fig. 1. Observation stations of study area. Circles and bold solid lines indicate CTD and ADCP observed station, respectively.

reduction in fishing grounds has led to the emphasis on formulations of alternative methods. In order to bring about changes to the fishing conditions and to develop a competitive fishing industry, the developing programs of fisheries resources, such as artificial reef programs, are being implemented in coastal zones (Lukens and Selberg, 2004; NFRDI, 2005; OECD, 1997; Seaman, 2000). An artificial reef was deployed in the South Sea, leading to the development of lower trophic levels, enabling the higher trophic levels to increase productivity.

The South Sea of Korea, bordered by the East/Japan Sea in the east, the Yellow Sea in the west, and the East China Sea in the south, is a coastal area in a continental shelf shallow than 100 m (Fig. 1). The coast is a rias coast consisting of many well–developed small islands, and water masses from the Tsushima Warm Current, a branch current of Kuroshio, are significant contributors to the region's fisheries oceanography (Choo and Kim, 1997). Further, the Tsushima Warm Current flows towards the coast lying east of the East China Sea, passes through Jeju's coast and into the South Sea, flows east parallel to the coastline and through the Korean Strait, finally emptying out to the East Sea (Chang, 1970; Lee and Cho, 1997). The tidal form number (F= K_1+O_1/M_2+S_2) was 0.11~0.17, suggestive of the more prominent semidiurnal tide (Odamaki, 1989).

Generally, due to the Tsushima Current passes at the South Sea of Korea, there is a lack of sources of cold water, resulting in higher sea surface temperature (SST) than in surrounding waters (Cho and Choe, 1988). Freshwater by direct rainfall or indirect from land affects salinity and turbidity in the South Sea of Korea. Freshwater flow from China's Yangtze River causes significant decreases in salinity levels of the South Sea of Korea (Beardsely *et al.*, 1992; Kim and Rho, 1994).

The purpose of this study is to confirm the existence of vertical flows originating from deployed artificial reef and to oberserve the variation of the water column. In addition, the variation of nutrients is studied after artificial reef deployment.

MATERIAL AND METHODS

The Shape of Artificial Reef and Observations

The material used for artificial reef construction was concrete as many of past cases did. A previous review's paper showed that concrete material was used almost 79 cases of total 309 citations with 17 different materials (Baine, 2001). Using 1 m concrete dice, an artificial reef (16~20×42×112 m) was constructed at the 5 km south–west of the Maemuldo (Fig. 2). The artificial reef in the study area, deployed from 2006 to 2008, is shaped like a small mountain range.

The size of the structure was changed throughout the observation period. In 2002, pre–deployment observation was begun, and in 2006, the artificial reef

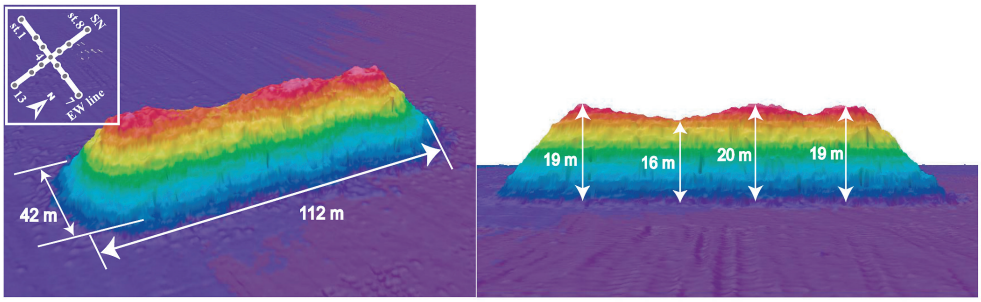

Fig. 2. Three–dimensional image of artificial reef using by MBS (Muti–beam Sonar).

(16~20×42×90 m) was deployed in water depth 55~65 m, and in 2007 and 2008, the length was increased by 10 m each year. In order to observe the impact of artificial reef, an observation station was set up by designating observation lines in 3 km radius from the center of artificial reef (St.4: 34.6° N, 128.5° E), since during a tidal cycle water mass travels about 6 km near the study area. Average water temperature, dissolved inorganic nitrogen (DIN), and dissolved inorganic phosphate (DIP) were measured before artificial reef deployment, on September 5, 2002 and after deployment, on August 28, 2006, July 30, 2007, and July 24, 2008. The measurements were taken at distances of 0.5 km, 1.5 km, and 3 km in radius, respectively, from the artificaial reef. Flood tides and ebb tides of both spring tide (July 23, 2008) and neap tide (July 30, 2008) were observed after the reef deployment during the summer of 2008. Sufficient data collection was difficult because of hindrances, such as the lack of or shortage of data before deployment in 2002, or bad weather conditions for carrying out the measurements in 2006 and 2007, when the structure had begun to develop into an artificial reef.

Water temperatures was measured every 0.5 seconds using a CTD (Conductivity Temperature Depth, SBE–19 SEACAT Profiler), and data represented in this study are outputs from 1 m intervals. Current measurements were carried out through line observation using the Acoustic Doppler Current Profiler (ADCP, RD Instruments Workhorse Mariner, 300 kHz). Line observation was selected, rather than observation from a fixed station, in order to be able to observe a larger area of current flow. It was found that there were factors affecting the acceleration of the boat during line observation, which ultimately affect the data collected, such as the shakiness of the boat due to waves, especially when winds cause relatively high wave heights (Kosro, 1985). In order to minimize such problems, the cruising speed was chosen to be about 7 knots after several trials, so that the effects of the boat speeding error on current measurements were minimized, taking the tide time into consideration. To minimize the positions' coordinate errors, the Differential Global Position System (DGPS) was combined with the ADCP program, enabling measurements in real time. The ADCP was configured to a bottom–tracking ping per second, and data were taken at either 10 s or 60 s intervals. In this case, the error ranges were 4 m for bin size (depth) and 10 s if the ensemble size (Δt) is 1.18 cm/s or 7.02 cm/s if 60s (RD Instruments, 1989).

Nutrients (DIN, DIP) measurements were taken from St.4 around the artificial reef. In locations near the center of the reef (Sts. 3, 5, 10 and 11), which were each 0.5 km from each other, samples were taken at 10 m depth intervals, and in locations 1.5 km or 3 km further from the center (Sts. 1, 2, 6, 7, 8, 9, 12 and 13), samples were taken from the surface, middle and bottom of three layers. Samples were collected using a Niskin sampler and then subsequently refrigerated in polyethylene bottles before further laboratory testing and analysis, following MOMAF regulations (MLTM, 2008; MOMAF, 2002, 2005 a.b, 2006, 2007).

Data Analysis

In the study area, tidal components of semidiurnal tides were prevalent, and as the main axis of the tidal current runs east–west, the artificial reef situated facing the north will most likely be affected by currents (Fig. 1) (Kim and Hwang, 2006a; Odamaki, 1989). Therefore, the environmental changes in study area were investigated by analyzing water temperature and nutrient levels from that of the east–west line, which was expected to be the most effective in representing current flow due to the artificial reef. In order to determine the changes of water temperature in summer thermoclines in this region before and after the reef deployment, water temperature data collected from CTD vertical profiling were analyzed.

In order to study the spatial variation of currents, horizontal current properties were used to analyze current direction and speed from the surface to lower layers and were represented with a vector time series. To investigate the spatial distribution of local upwelling flow (hereinafter called LUF) and local downwelling flow (hereinafter called LDF), velocity components were diagrammed versus depth. To remove noise, such as short period waves, low–pass filtration was used. Although low–pass filtration cannot remove spatial differences or components due to discontinuous tidal currents, it is capable of removing short period components. The cutoff frequency was set to 0.2 cycles per minute (Emery and Thomson, 2001).

To determine the degree of vertical mixing due to the artificial reef, the current shear (S) (Mack and Hebert, 1999) was calculated using the ADCP horizontal current component, as shown in Equation 1,

$$S=\sqrt{\left(\frac{\partial u}{\partial z}\right)^2+\left(\frac{\partial v}{\partial z}\right)^2} \quad (1)$$

where u and v represent east–west and north–south components, respectively, and z, the ADCP depth interval, is 4 m. During the summer, when sunlight is strong, pycnoclines are formed, but artificial reef weakens the pycnocline by causing changes in water temperature and salinity distribution. In addition, turbulence due to current shears from the artificial reef destroys stratification, and the stability of the water column was determined by calculating energy required, represented by the Richardson number (Ri). The Richardson number was calculated using current shear (S) and the Brunt–väisälä frequency N as in Equation 2,

$$Ri=\left(-\frac{g}{\rho}\frac{\partial \rho}{\partial z}\right)\Big/\left(\frac{\partial U}{\partial z}\right)^2=\left(\frac{N}{S}\right)^2 \quad (2)$$

where N ($=\sqrt{-g/\rho\left(\frac{\partial \rho}{\partial z}\right)}$) describes the strength of the

stratification; g represents gravitational acceleration; ρ is density; z is depth; and U is horizontal velocity. If the $Ri>0.25$, the water column was considered to be stable (Rippeth, *et al.*, 2005; van Haren, *et al.*, 1999), while $Ri<0.25$ indicated instability due to turbulence (Miles, 1961). The Brunt–väisälä frequency (N) describes the strength of the stratification, and as the density gradient increases, the restoration force of N becomes stronger, along with increasing oscillation number and decreasing oscillation period. Hence, the greater the stability of stratification, greater is the frequencyand, therefore, the oscillation period decreases, resulting in a greater value of N (Pickard and Emery, 1990).

The changes in vertical distribution of nutrients (DIN, DIP) due to the artificial reef were determined by using objective interpolation carried out by MLTM (2008) and MOMAF (2002, 2005a.b, 2006, 2007).

RESULTS

Variations of Water Temperature Distribution

The effects of the artificial reef on water temperature distribution during stratification were examined by studying the vertical distribution of water temperature during the summer, before and after deploying the reef (Fig. 3). First, in order to characterize the spatial variation of the thermoclines due to the reef, the maximum thermocline through the water column (hereinafter called MTWC), where the vertical gradient of water temperature (dT/dz, T: temperature, z: depth) is steepest, was studied (Kirinich and Hebert, 2005).

The vertical distribution of water temperature was observed on September 5, 2002, before the deployment of the artificial reef. As figure 3(a) shows, the range of water temperature 17.0~24.5°C, with most rapid changes in depths of 20~40 m and strong thermocline was formed in depths of 35 m. In a region about 2~3 km west from St.4, thermocline depth rose about 10 m than that of the neighboring regions. This shows that the eastern regions of the study area are deep and become successively shallower towards the west (Sts. 1~3), indicating the topographic changes due to increases in water temperature. With the exception of such localized water temperature, the region's MTWC during the summer formed uniformly in depths of 30~40 m.

According to data from August 28, 2006, after deployment, the range of water temperature from the lowestlayer to the surfacelayer was about 13°C, from 14.5~27.5°C (Fig. 3(b)). On the western side of the artificial reef (St. 4), the MTWC formed in depths of about 20 m, increasing gradually to about 25 m with decreasing distance from the artificial reef. On the eastern side of the artificial reef, on the other hand, the depth of the MTWC suddenly became about 10 m shallow, continu-

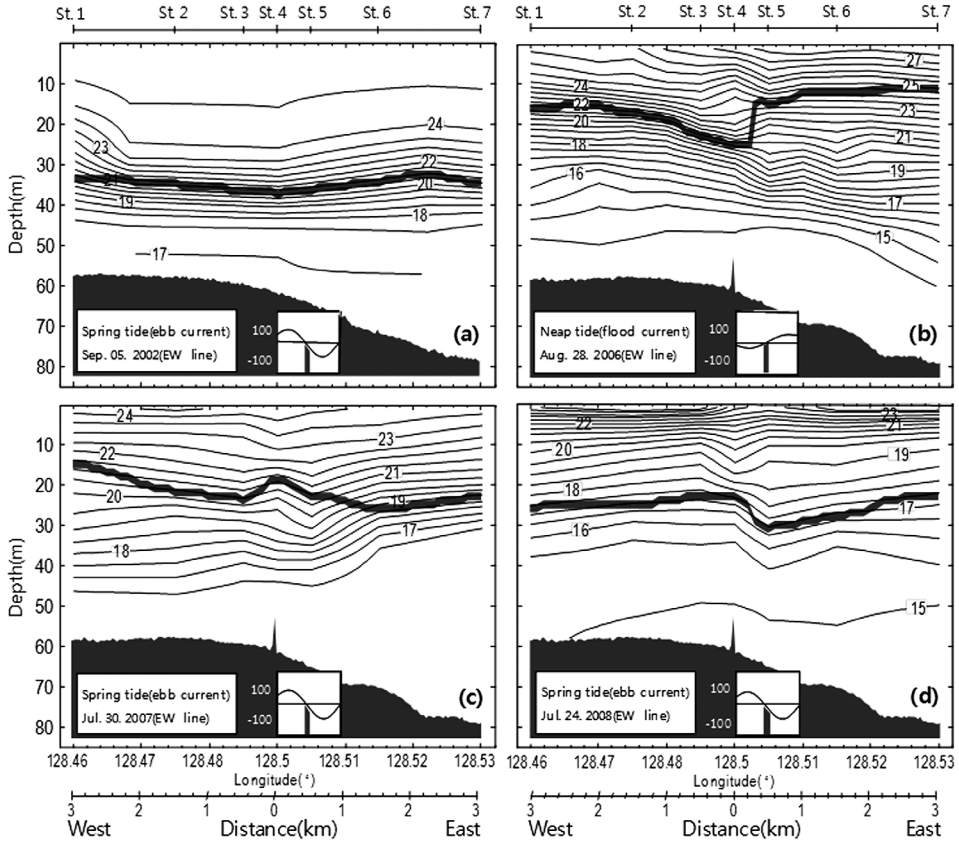

Fig. 3. Cross section of temperature obtained by CTD observation on September 5, 2002(a), August 28, 2006(b), July 30, 2007(c) and July 31, 2008(d). Shading lines indicate differential maximum temperature divided by depth. Contour intervals are shown every 0.5°C.

ing to a distance of about 3 km. The vertical water temperature profile from July 30, 2007 (Fig. 3(c)) showed that the surface layer had high water temperatures, at 24.5℃, however, the lower layer had water temperatures about 16.5℃. The depth of the MTWC at St. 1, about 3 km west from the artificial reef, was about 15 m, and the depth increased gradually with nearing distance from the reef to about 23 m. However, the formation depth of the MTWC suddenly became shallower by 5 m in areas 1 km from the reef, forming a dome–shape. Then, the depth increased again to about 25 m with increasing distance towards the east. The MTWC runs about 25 m from the west to the artificial reef and at sts. 5 and 6, situated about 0.5~1.5 km east of the reef, the depth dramatically increased to about 33 m and then gradually became shallower with increasing distance, ultimately showing similar to depth change that of the western region. Hence, after comparison of the MTWC formation depths from before and after deployment of the reef, the depth varied by about 5 m before deployment, while the variation grew to about 10~17 m after the deployment, showing about 2~3 times greater difference. In addition, the thermocline formation depth on east of the reef center (St. 4) varied from that of the west after the artificial reef deployment, showing concavity changes between flood tide and ebb tide (Figs. 3 (b), (c), and (d)).

Horizontal Currents Distribution near the Artificial Reef

The properties of horizontal currents surrounding the artificial reef were characterized by studying the vertical profiling of spring and neap tides, along with flood and ebb tides (Fig. 4). Vertical profiling during spring (July 23, 2008) flood tide's horizontal current properties showed that the southwestward flow and northwestward flow existed in areas near the surface layer, at depths of 7 m, but in areas 15~31 m deep, the southwestward flow was prevalent (Fig. 4(a)). However, in areas of depths 39 m, a boundary layer formed showing spatialy different directions of flow between the northwestern and southwestern components, and in areas deeper than 39 m, the northwestward flow showed to be prevalent. The southeastward flow showed to be prevalent in all areas during ebb tide, except in depths of 3~39 m, where the southeastward flow decreased, and a mixed loading between the northwestward and southwestward flows could be seen. The southeastward flow became more dominant again near the bottom, in depths of 47 m, and was especially significant in depths of 55 m in western areas. Relatively strong currents in the lower layer are due to the fact that the area is situated at the top of a continental shelf, and this phenomenon can be described to be characteristic of strong tidal currents flowing from deeper to shallower areas (Mann and Lazier, 1991).

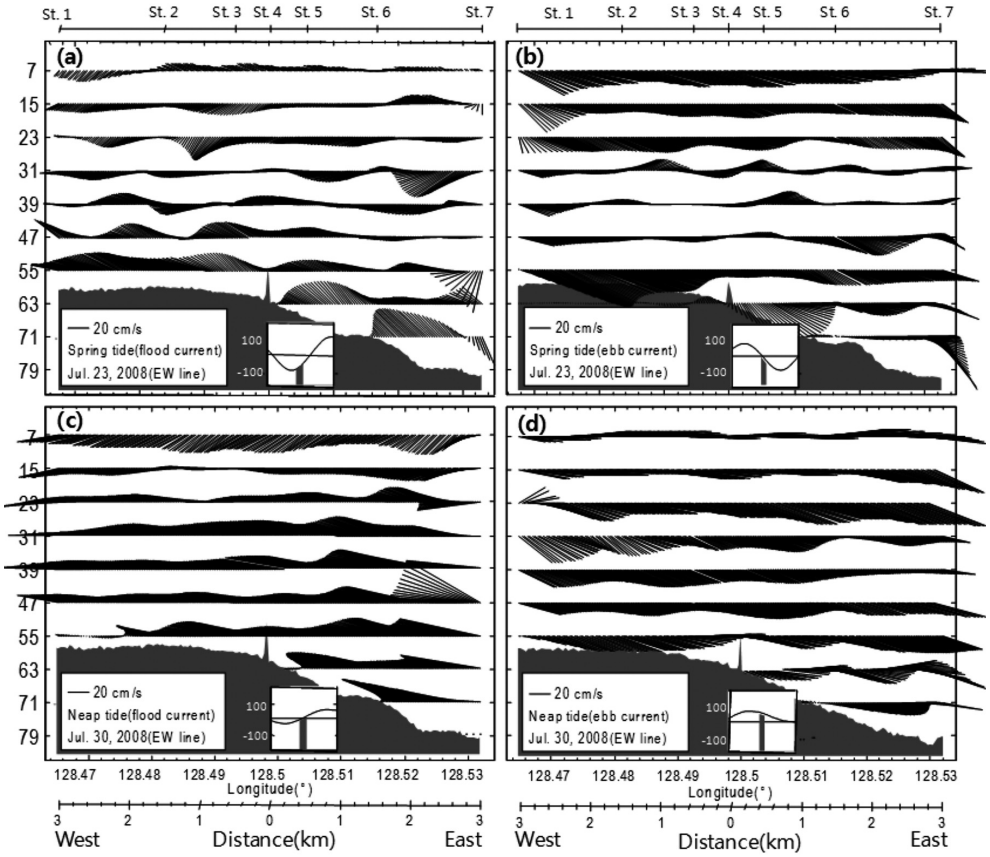

Fig. 4. Stick vector plot of low–passed velocity at spring and neap tide on July 23, 2008(a, b) and July 30(c, d) 2008. Observed from flood currents (a) and (c), and ebb currents (b) and (d).

Horizontal current profiles by depth, collected during neap (July 30, 2008) ebb tide, showed that in areas of depth 15 m in the surface layer, the southwestward flows were dominant, and in depths of 23 m, a mixed water mass bysouthwestward and northwestward flow could be seen (Fig. 4(c)). However, in areas deeper than 23 m, unlike in the upper layers, where the southwestward flows were dominant, the horizontal current components showed to be predominantly northwestward, the speed increasing with proximity to the bottom layer. In addition, the ebb tide current distribution reflected with the exception of the surface layer, the southeastward flow was dominant throughout all depths (Fig. 4(d)). Thus, the horizontal component showed to be predominantly mild southwestward and northwestward flow in depths of 7 m, while in areas 15 m towards the bottom layer, current flow became increasingly predominantly southeastward.

The study area's main tidal direction was northwestward at flood tide and southeastward at ebb tide (Kim and Hwang, 2006a). Vertical profiling of the horizontal current component was dependent on depth at both flood tide and ebb tide. During spring tide, the boundary layer between the surface and bottom layers was at 31~39 m in depth, while it was at 15 m in depth during neap tide. During flood tide, the direction of the southwestward flow in the upper layer and the northwestward flow in the lower layer changed, based on the boundary layer, but during ebb tide, the southeastward and northeastward flows coexisted, with the layer below the boundary layer showing stronger southeastward flow than that of the upper layer.

Vertical Currents Distribution near the Artificial Reef

Due to strong horizontal currents from the lower layer, it will be possible for LUF and LDF to arise. In order to characterize spatial distributions of LUF and LDF after the artificial reef deployment, depth–dependent vertical currents during spring and neap tides (July 23, 2008 and July 30, 2008) were studied (Fig. 5).

The flood tide distributions during spring (July 23, 2008) tide showed that overall, LUF was predominant (Fig. 5(a)). The LDF was evident 200 m west (St. 4) of the artificial reef, and LUF was present strongly to areas 1 km on both sides depending on current directions. The LDF appeared in areas shallower than 20 m, about 2.5 km west and 1 km east of the artificial reef, and the strength was weaker than that of LUF. Likewise, LUF was stronger in ebb tide distributions, showing to be strongest 1 km the east and west of the artificial reef and also in regions between 2 and 3 km to the east of the artificial reef (Fig. 5(b)). On the other hand, LDF appeared about 2 km to the west and 1.6 km to the east of the artificial reef, but it was evident that the LDF regions had moved eastward relative to those of spring flood tides. During neap (July 30, 2008) flood tides, vertical current distributions showed that LUF and LDF

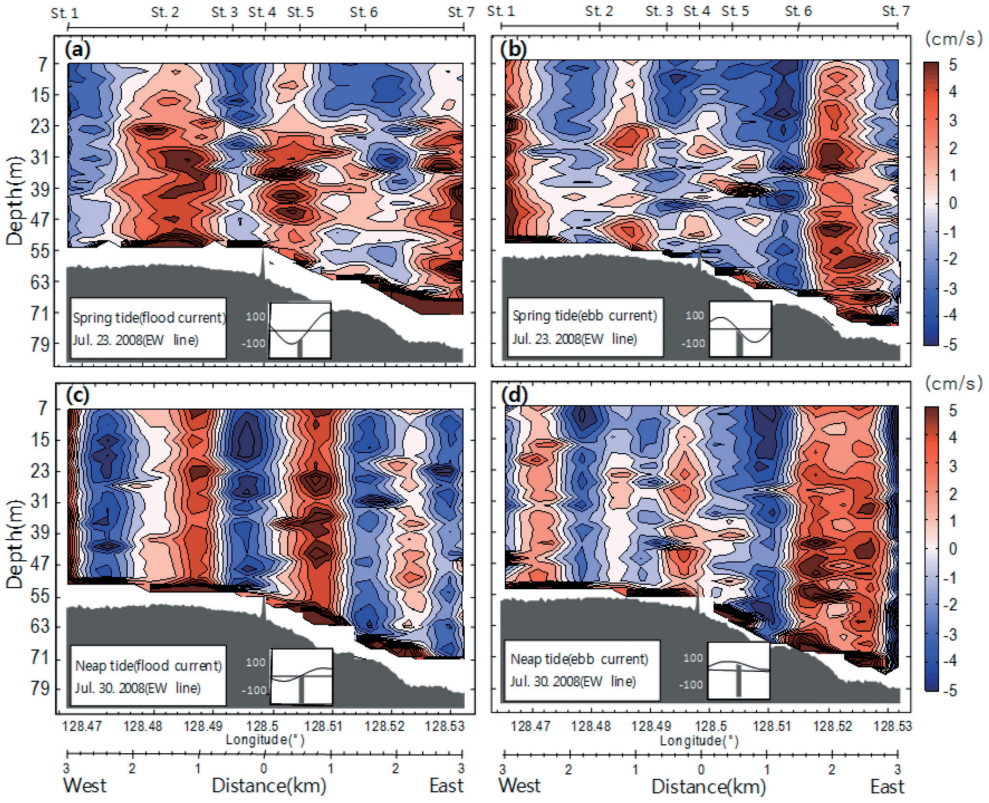

Fig. 5. Vertical distribution of w–component at spring and neap tide on July 23, 2008(a, b) and July 30(c, d) 2008. Observed from flood currents (a) and (c), and ebb currents (b) and (d). (red: LUF and white: LDF).

formed alternating columns (Fig. 5(c)). Although the strength of the LUF varied in areas about 1 km to the west and 1 and 2 km east of the artificial reef, the LUF was still present in all depths. The ebb tide LUF distributions showed similar alternating patterns between LUF and LDF during flood tides, but the strength was less than that of flood tide time (Fig. 5(d)). About 2 km east of the artificial reef was an area about 1 km in diameter with very strong LUF, and the LDF appeared about 1 km more eastward. Thus, there were tide time–dependent variations in vertical current distributions around the artificial reef, in which there were spatial variations in LUF and LDF. Finally, the alternating columnar pattern between LUF and LDF was clearer during neap tides than in spring tides, depicting the temporal and spatial variations.

Currents Shear near the Artificial Reef

In order to study the spatial distribution of vertical mixing in areas surrounding the artificial reef, shear was calculated (Fig. 6). According to the vertical profiles of spring (July 23, 2008) flood and ebb tides, the distribution of flood tide around the reef area (St. 4) showed to have large current shear in depths of 15~40 m (Fig. 6(a). However, when compared to either side of the artificial reef, the top layer showed to have weaker current shear, indicating that the strength of current shear varies with spatial variation. The ebb tide current shear distribution showed similar patterns as that of flood tide, but the region of strong current shear in the middle of the artificial seamount showed to be a wider area than that of flood tide (Fig. 6(b)). On the other hand, the current shear of neap (July 30, 2008) flood tide was not as strong as that of spring flood and ebb tide or neap ebb tide, but regions near the surface layer, at depths 7~30 m, had stronger current shear than that of surrounding areas (Fig. 6(c)). Likewise, lower layers also exhibited strong partial current shear around the artificial reef (Fig. 6(d)). During ebb tide, strong current shear was visible in depths of 23~31 m to the east and west of the artificial reef, as well as a pattern of alternating strong and weak current shear regions. This phenomenon depicts the effects of the artificial reef on horizontal current shear in surrounding areas, and the distribution parallels that of the LUF and LDF in this area (Fig. 5). On the whole, however, as the calculated bottom layer's strong current shear during spring and neap flood and ebb tide can largely be attributed to the friction due to the current's lower topography and most likely has no relationship to the effects due to the artificial reef (Mann and Lazier, 1991).

Distribution of Richardson Number in Regions Surrounding the Artificial Reef

The stability of the coastal sea layers under the influence of the strong summer solar radiation is quite different from that of the winter, when the seas are influenced largely by wind or tide. The water column stabil-

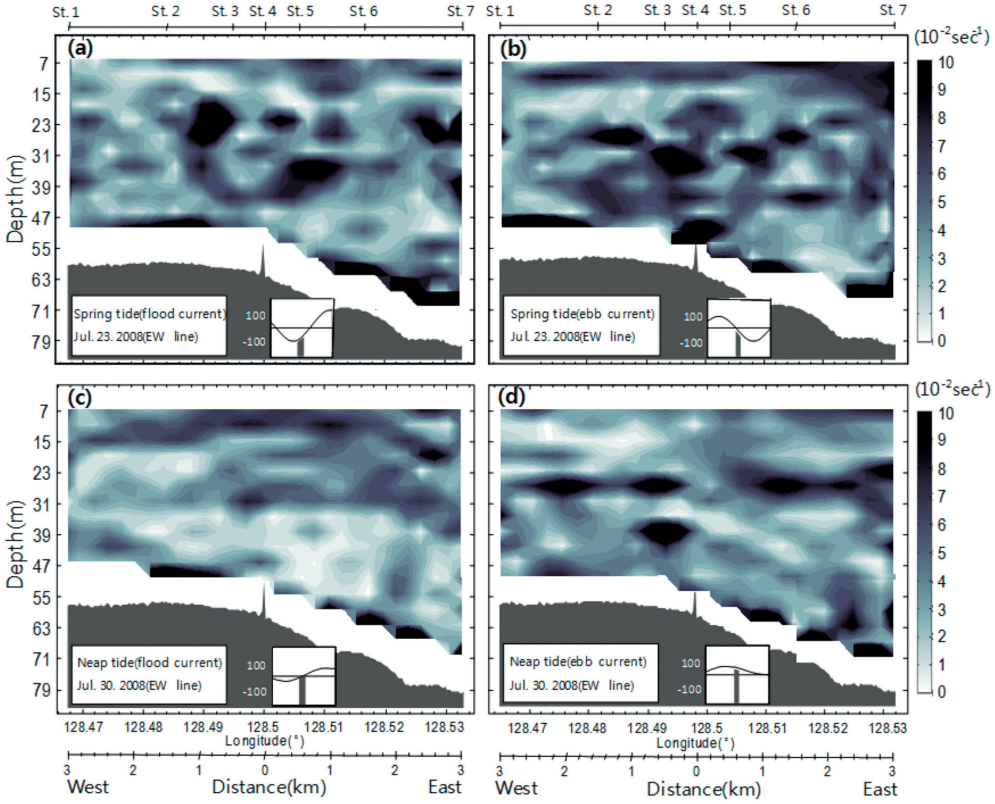

Fig. 6. Vertical shear contours computed from ADCP measurements at spring tide on July 23, 2008(a, b) and at neap tide on July 30(c, d) 2008. Observed from flood currents (a) and (c), and ebb currents (b) and (d).

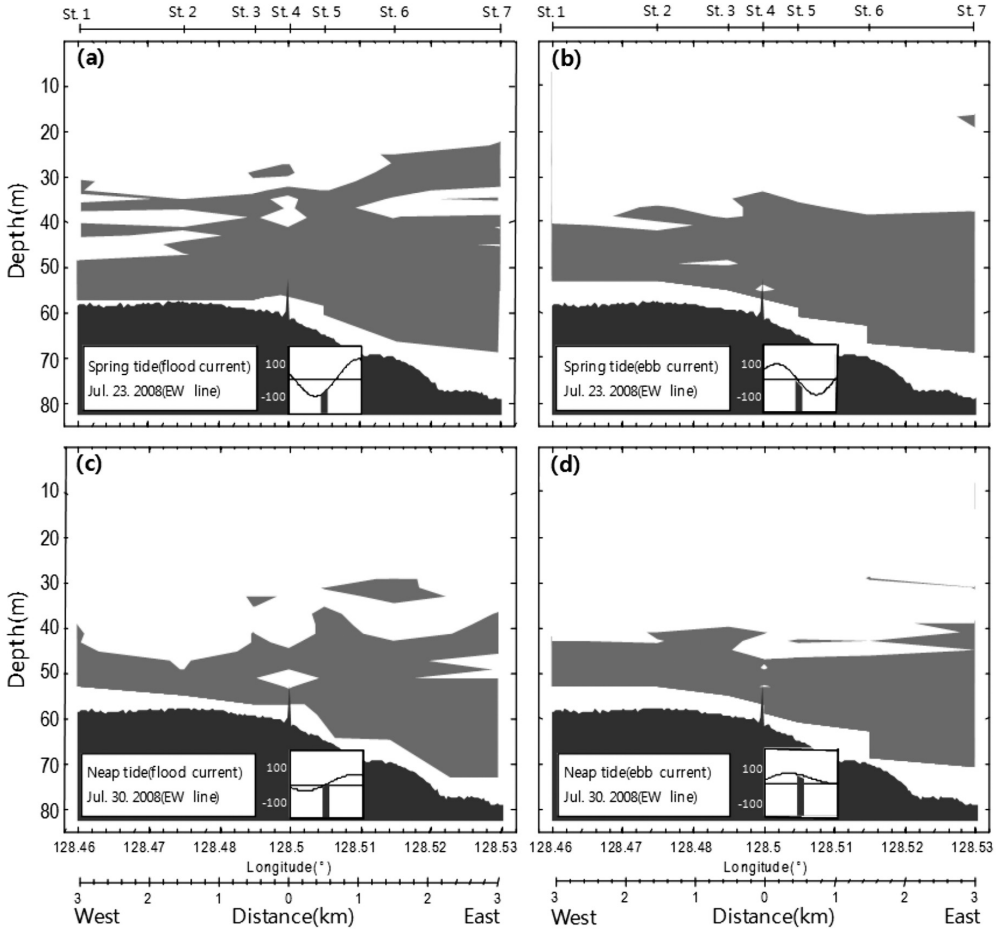

Fig. 7. Vertical distributions of Richardson number at spring and neap tide on July 23, 2008(a, b) and July 30(c, d) 2008. Observed from flood currents (a) and (c), and ebb currents (b) and (d). The white and shaded represent $Ri>0.25$, $Ri<0.25$ regions, respectively.

ity of the area surrounding the artificial reef was determined by using the vertical distribution of Richardson number (Ri) during the summer of 2008 (July 23 and 30) (Fig. 7). As figure 7 shows, regions with $Ri<0.25$ had an unstable water column, while those with $Ri>0.25$ had a stable water column. While optimal conditions require data collection at the same time, due to turbulences in the sea state, simultaneous collection of values such as current speed, water temperature, salinity, and density was difficult. Some data were collected a day later, but to minimize differences, data from the same tide time were used. According to the spring flood tide vertical distribution of Ri, areas to the west of the artificial reef, with depths less than 30 m, had a stable water column distribution ($Ri>0.25$), and areas to the east, in depths about 10 m shallower than in the west, had a stable water column (Fig. 7(a)). In deeper areas to the east and west of the artificial reef, $Ri<0.25$ was indicative of unstable water columns. During ebb tide, layers above 30~40 m had stable water columns, with $Ri>0.25$, and layers below had an unstable water column distribution, with $Ri<0.25$ (Fig. 7(b)). According to neap tide distributions, except in areas in depths of 30 m, all other areas to the east of the artificial reef in layers shallower than 40 m had $Ri>0.25$, indicating stable water columns (Fig. 7(c)). Depths deeper than 40 m showed an unstable distribution of water columns, with $Ri<0.25$. During ebb tide, the water column stability, with respect to depths of 40 m, increases with proximity to the surface layer and decreases towards the bottom (Fig. 7(d)).

In summary, areas in layers above depths of 30~40 m had a stable distribution of water columns, with $Ri>0.25$, while layers below depths of 30~40 m showed unstable water columns, with $Ri<0.25$. Such variations in water column stability can be attributed to a gradient in continental shelf morphology, as well as to vertical currents due to the artificial reef. As in the study region, areas that achieve water layer stability during summer stratification become unstable not only as a result of vertical diffusion due to bottom friction, but also because of vertical mixing due to LUF and LDF due to the artificial reef.

Variation in Nutrient Distribution

Vertical currents originating around the artificial reef generate vertical mixing, and this process causes variations in the region's water column stability. Thus, in order to study the summer nutrient distribution around the artificial reef, vertical structures of DIN and DIP before and after the artificial reef deployment were compared. According to the vertical structure of DIN

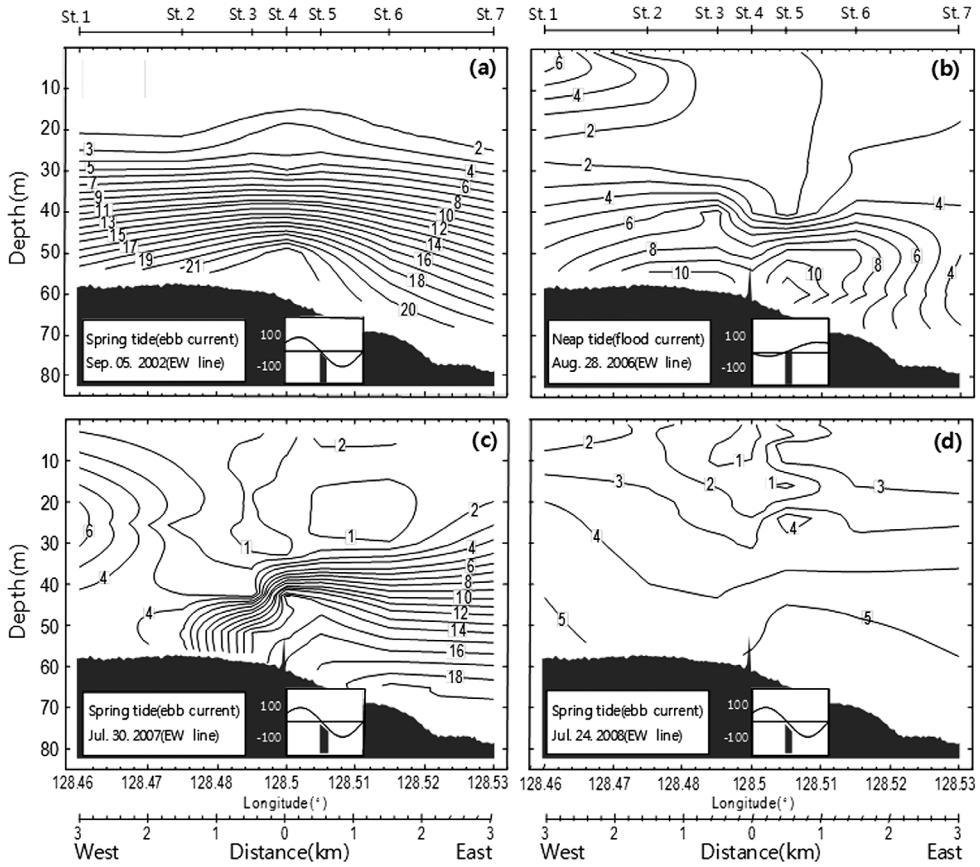

Fig. 8. Vertical distributions of DIN on September 5, 2002(a), August 28, 2006(b), July 30, 2007(c) and July 31, 2008(d) (unit : μM).

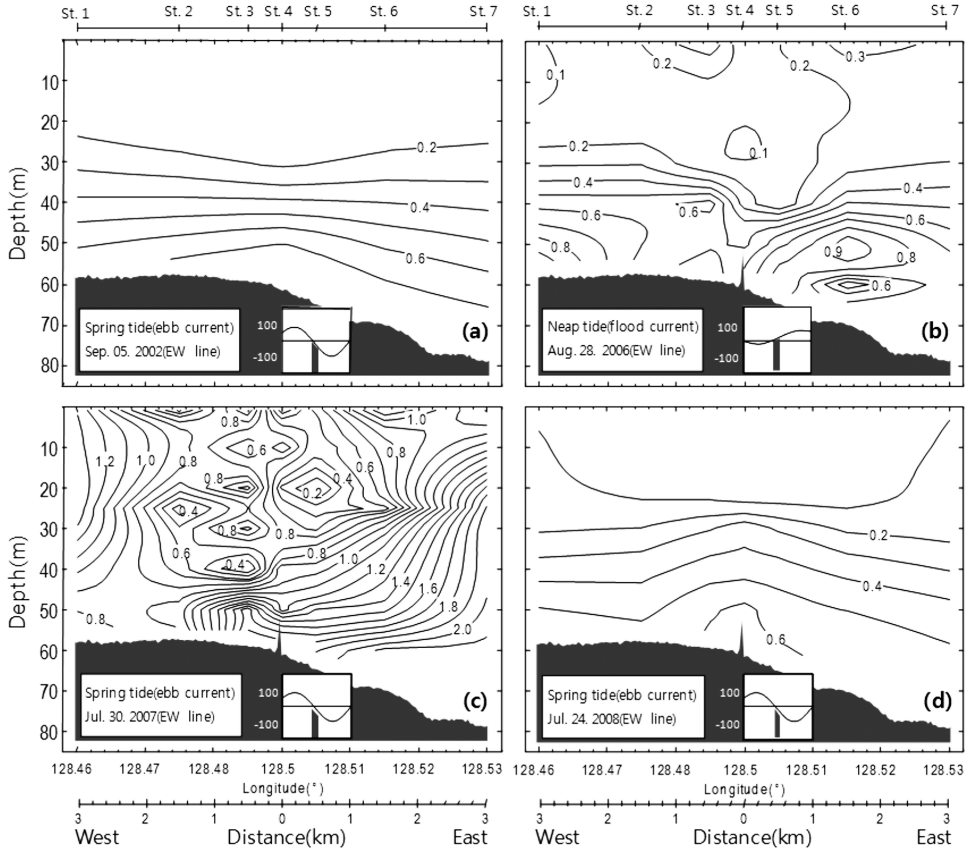

Fig. 9. Vertical distributions of DIP on September 5, 2002(a), August 28, 2006(b), July 30, 2007(wc) and July 31, 2008(d) (unit : μM).

before deployment (September 5, 2002), the concentrations ranged from 2.0~20.0 μM, increasing from the surface to the bottom layer (Fig. 8(a)). Likewise, the DIP concentration, ranging from 0.2 μM in the surface layer to 0.7 μM in the bottom layer, showed higher concentrations in the bottom layer than in the surface layer (Fig. 9(a)). Thus, nutrient levels during summer stratification before the artificial reef deployment showed to have an uniform pattern, with low concentrations in the surface layer and high concentrations in the bottom layer.

According to the vertical structure of DIN after deployment (August 28, 2006), the concentrations ranged from 0.5~11.0 μM averaging 4.0 μM through the water column (Fig. 8(b)). There was an area about 1~3 km to the west of the artificial reef near the surface layer (up to about 20 m in depth) with a slightly high concentration (2.0~6.0 μM), but in general, areas with depths 30 m or shallower had relatively low concentrations (2.0 μM) increasing to the bottom layer. In particular, the upper portion of the artificial reef, in depths of 40~50 m, had high concentrations of DIN (7.0~10.0 μM). In addition, about 1.5 km west from the artificial reef was an area in depths below 50 m with high concentrations of DIN.

The average DIP concentration in the region was 0.3 μM, ranging from 0.1~0.9 μM (Fig. 9(b)). Part of the surface layer had low concentrations of 0.2~0.3 μM, but from depths of 30 m, the concentrations became higher with increasing depth. About 1.0~2.5 km to the east of the artificial reef was an area with high concentrations (0.9 μM), and in general, the distribution of DIP concentrations showed a similar pattern as that of DIN concentrations. According to DIN distribution data from July 30, 2007, the following summer, the concentrations ranged from 2.0~20.0 μM, showing higher concentrations with increasing depth (Fig. 8(c)). From St. 4, where the artificial reef is located, the DIN accumulated the upper on area of the reef, and to the right of the reef, the high concentration of DIN in the bottom layer was noted to rise to the upper layer. The concentration of DIP ranged from 0.2~2.0 μM throughout the layers. There was a high concentration (1.0 μM) in an area about 1.0 km to the west of the artificial reef in depths below 45 m, and the distribution of high concentrations increased towards the east of the artificial reef, depending on depth, so that DIP concentrations of 1.0 μM in an area 3.0 km to the east of the artificial reef had risen to depths of 10 m. In 2007 and 2008, especially, an area 1.0~3.0 km to the west of the artificial reef, in depths of 40 m, had a high nutrient concentration, but because this area is located near the land and was likely temporarily influenced by sources from the land, further investigation may be necessary. According to DIN distributions from July 24, 2008, the average concentration was 3.2 μM, with a total range of 0.5~5.0 μM (Fig. 8(d)).

The surface layer of St.4 or the center of the artificial reef, there was a low concentration of DIN in depths of 10 m, but the concentration increased with increasing depth. The average DIP concentration was 0.2 μM, ranging from 0.1~0.6 μM throughout the layers (Fig. 9(d)). The distribution of DIP concentration, which showed higher density with increasing depth, showed relatively high concentrations (0.6 μM) in areas 1.0 km around the artificial reef, showed to have uplifted to 30 m, forming a dome shape. The concentration of DIN was lower in the summer of 2008 compared to previous years (2002, 2006, 2007), but nevertheless, comparison of data before and after the artificial reef deployment shows that there are changes in DIN distributions. Hence, it can be noted that there is a clear difference in summer nutrient levels before and after artificial reef deployment, and from observing data. It is apparent that the variation of nutrient levels is not limited to a year, but, rather, a persistent happening.

DISCUSSION

Obstacles such as the artificial reef deployed on the sea floor have significant impacts on water temperature distribution during summer stratification. In this study, the MTWC formation depth was about 35 m before the artificial reef deployment, with a small degree of vertical variation (Cho *et al*., 2003; Kim and Hwang, 2006a). In regions about 1 km around the artificial reef, changes in MTWC depth were seen, ranging from 10 to 17 m, depending on tide time (Fig. 3). Such a phenomenon, in which obstacles such as cause thermal uplifting, has also been observed in the Porcupine Bank of the Irish continental shelf (Mohn *et al*., 2002; Mohn and Beckmann, 2002), the Fieberling and Horizon Guyots of the Pacific Ocean (Genin *et al*., 1989), the Cobb Seamount (Freeland, 1994; Dower and Mackas, 1996). However, due to the scale difference comparing to natural seamount, isothermal uplifting wasn't observed.

Generally, on flat sea floors, the strength of surface layer currents weakens near the sea floor because of frictional force from the floor. However, in the study area, horizontal current velocities between upper layer and bottom layer have opposite directions, with respect to the boundary depth. There were strong currents even in the bottom layer of this region (Fig. 4). Hence, in areas neighboring artificial reef, it is difficult to determine solely the depth–related influence of the artificial reef on horizontal currents. As this region is located at the edge of the continental shelf, from which semidiurnal currents arise easily (Odamaki, 1989), the changes in surface and bottom layer current flow should be determined from this region's current properties (Cho *et al*., 2003). It must be kept in mind, however, that vertical currents like LUF and LDF arise around artificial reef, with spatial differences in current origin according to tide time. In other words, LDF arises at the top of the artificial reef, and strong LUF are seen on the sides of the artificial reef, and the pattern of such currents varies spatially depending on whether it is spring or neap tide, and flood or ebb tide (Fig. 4). Vertical currents arising from around the artificial reef, such as LUF or LDF, cause turbulence when combined with the vertical water mass, uplifting the thermocline. Thus, the strong vertical currents of LUF arise from obstacles such as

artificial reef (Skyllingstad and Wijesekera, 2004) and consequently result in changes in marine environments. Areas with strong current shear were regions from which LUF and LDF originate, and it was noted that there were similar spatial distributions. These regions were about 1~2 km in width and were located on either side of the artificial reef (Fig. 6). The water column in the artificial reef area had $Ri<0.25$ in depths of deeper than 30~40 m, indicating that the column was unstable (Fig. 7). According to Owens and Hogg (1980), the low water column stability around a 400 m high natural seamount in the Gulf Stream is due to the upwelling flow that arises from regions with strong current shear. In this study, as well, it can be seen that obstacles on the sea floor, such as the artificial reef, result in such instability of the water column. Artificial reef destroyed strong stratification during the summer because vertical currents such as LUF and LDF arise as a result of obstacles on the sea floor, resulting in thermocline uplifting. The vertical currents caused by artificial reef lead to vertical mixing and enhance instability of the water column in areas surrounding artificial reef.

In general, inorganic nutrients are more abundant in the aphotic zones, where they are not consumed as much as in the euphotic layer (Caffrey *et al*., 2007; Markaki *et al*., 2010). During the summer, especially, when stratification is strong, vertical mixing between surface and bottom layers is weak, causing much of the nutrients to accumulate in the lower layers (Mann and Lazier, 1991).

According to observations of the nutrients (DIN and DIP) distribution before deployment in areas surrounding the artificial reef, there is a low concentration of nutrients in the surface layer, while the lower, aphotic zones of the coastal areas during the summer have a high concentration of nutrients. After the artificial reef deployment, however, with the exception of a few temporal and spatial differences, the nutrients showed to be concentrated by the upper portion of the artificial reef, in depths of about 30~40 m (Figs. 8 and 9). Such difference is due to vertical mixing resulting from LUF around the artificial reef, which causes the water column to become unstable, consequently uplifting the high concentration of nutrients during the summer.

According to numerical calculation of the resident time by material obstacles, such as seamounts, the particle follows a uniform cyclonic tidal current, forming a Taylor column and consequently prolonging the resident time (Goldener and Champman, 1997). Mullineaux and Mills (1997) studied the summer Fieberling Guyot, located in the northeastern Pacific, and found that when there is steady flow or tidal current, the particle damages are smallest. The areas surrounding the artificial reef in the study area are influenced by obstacles on the sea floor, stratified water column, steady flow, and tidal current (Cho *et al*., 2003; Kim and Hwang, 2006a.b). Likewise, in areas surrounding the artificial seamount, the resident time of particles becomes longer, resulting in less damage of particles such as nutrients and thus an abundant accumulation of nutrients (Mullineaux and Mills, 1997). As it is possible to see that there is an abundant accumulation of nutrients on the Cobb seamount (Dower *et al*., 1992) or Porcupine Bank (White *et al*., 1998) from isothermal/isopycnal domes that arise in the upper portions of seamounts, dynamic qualities of artificial seamounts, such as LUF, cause changes in thermoclines, leading to increased productivity.

The abundant nutrients lead to increased plankton biomass (White *et al*., 2004). In addition, strong vertical shear around the Emperor Seamount in the northern Pacific (Roden and Taft, 1982) or the EBES (*El Bajo de Espiritu Santo*) seamount in California (Trasviña–Castro *et al*., 2003) cause dynamic instability of water columns, which increases primary productivity of the euphotic layer, as well as the increase in variety of species (Pingree *et al*., 1975). The artificial reef was deployed at about 55~65 m in depth, and coastal regions with strong currents, depths until 30 m can be regarded as the euphotic layer (Mann and Lazier, 1991). The artificial reef located in the study region is smaller than most natural seamounts, with a size of about $6.0\times10^4 m^3$. For example, compared to the EBES seamount, with an area of about $6.0\times10^7 m^3$ (Trasviña–Castro *et al*., 2003), the artificial reef in the study area is about 10^3 times smaller. Despite its smaller size, the artificial reef can nevertheless cause the same increases in primary productivity through environmental changes like isotherm dome due to water column instability or current shear, which cause provide abundant nutrients to the euphotic layer (Yanagi and Nakajima, 1991). Thus, in the South Sea of Korea, which has an artificial reef above a continental shelf, is capable of causing strong semidiurnal tidal currents (Odamaki, 1989), due to turbulence from the strong bottom friction (Simpson *et al*., 1982) in the natural state. Such currents are capable of causing strong vertical mixing from LUF due to the artificial reef, which, in turn, leads to the smooth distribution of the abundant nutrients in the bottom layer to the upper layers.

According to the environmental conditions that have been considered thus far, it is important for the area to have strong stratification, with strong current velocities arising as a result of obstacles in the bottom layer (Yanagi and Nakajima, 1991), in addition to an appropriate sea floor topography taking the sinking rate into consideration (Jeon *et al*., 2007). In order to form a fishing environment with high primary productivity in coastal areas by deploying an artificial reef, the type of sea area chosen for artificial reef deployment must have optimum environmental conditions, above all.

ACKNOWLEDGEMENTS

This work has been supported by the Korea Institute of Planning & Evaluation for Technology in Food, Agriculture, Foresty & Fisheries (iPET).

REFERENCES

Baine, M. 2001 Artificial reefs: a review of their design, application,

management and performance. *Ocean & Coastal management*, **44**: 241–259

Barber, R. T. and W. O. Smith 1981 Coastal upwelling ecosystem. In "Analysis of Marine Ecosystems", ed. A. R. Longhurst, London: Academic, 31–68

Beardsely, R. C., R. Limeburner, K. Kim and J. Candela 1992 Lagrangian flow observations in the East China. Yellow and Japan Seas, *La mer*, **30**: 297–314

Boje, R. and M. Tomczak, (Ed), 1978 Upwelling Ecosystems. Springer–Verlag, p. 303

Caffrey, J. M., T. P. Chapin, H. W. Jannasch and J. C. Haskins 2007 High nutrient pulses, Tidal mixing and biological response in a small California estuary: Variability in nutrient concentrations from decadal to hourly time scales. *Estuarine, Coastal and Shelf Science*, **71**: 368–380

Chang, S. –D. 1970 Computation of Wind Drift Currents in the Southern Waters of Korea. *Bull. Korean Fish. Soc*, **3**: 199–206

Cho, K. –D., D. –S. Kim and S. –E. Park 2003 Characteristics of Oceanographic Conditions in an Area Suitable for the Construction of Artificial Upwelling. *Bull. Korean Fish. Soc*., **36**: 187–192

Cho, K. –D. and Y. –K. Choe 1988 Seasonal Variation of the Water Type in the Tsushima Current. *Bull. Korean Fish. Soc*., **21**: 297–306

Choo, H. –S. and D. –S. Kim 1997 The Effect of Variations in the Tsushima Warm Currents on the Egg and Larval Transport of Anchovy in the Southern Sea of Korea. *Bull. Korean Fish. Soc*., **31**: 226–244

Chung, C. –S. and D. –B. Yang 1991 On the primary productivity in the southern sea of Korea. *J. Oceanol. Soc. Korea*, **26**: 242–254

Cushing, D. H. 1969 Upwelling and fish production. F. A. O. Fish. Tech., 84, p. 38

Cushing, D. H. 1971 Upwelling and the production of fish. *Adv. Mar. Biol*., **9**: 255–334

Dower, J., H. Freeland and K. Juniper 1992 A strong biological response to oceanic flow past Cobb seamount. *Deep–Sea Research*, **39**: 1139–1145

Dower, J. and D. L. Mackass 1996 "Seamount effects" in the zooplankton community near Cobb Seamount. *Deep–Sea Research*, **43**: 837–858

Emery, W. J. and R. Z. Thomson 2001 Data analysis methods in physical oceanography. Elsevier, Second and Revised Edition, p. 328

FAO 1998 Fishery country profile–Republic of Korea. Food and Agriculture Organozation of the United Nations (FAO), Rome, Italy, Report No. FID/CP/ROK

Freeland, H. 1994 Ocean circulation at Cobb seamount. *Deep–Sea Research*, **41**: 1715–1732

Genin, A., M. Noble and P. F. Lonsdale 1989 Tidal currents and anticyclonic motions on two North Pacific seamounts. *Deep–Sea Research*, **36**: 1803–1815

Goldner, D. R. and D. C. Chapman 1997 Flow and particle motion induced above a tall seamount by steady and tidal background currents. *Deep–Sea Research*, **44**: 719–744

Jeon, Y. H., G. S. Lee, Y. K. Kang and C. R. Ryu 2007 An Experimental Study for the Falling Test and Upwelling Effect of the Artificial Upwelling Structures in Flow Field. *J. Oceanol Engi. Tech*., **21**: 21–27

Kim, D. –S. and S. –B. Hwang 2006a Characteristics of Oceanographic Environment in A Sea Area for the Building of Artificial Upwelling Structure. *Journal of the Korean Society of Marine Environment and Safety*, **12**: 1–8

Kim, D. –S. and S. –B. Hwang 2006b The Variation of Current by the Building of Artificial Upwelling Structure (1). *Journal of the Korean Society of Marine Environment and Safety*, **12**: 301–306

Kim, I. –O. and H. –K. Rho 1994 A Study on China Coastal Water Appeared in the Neighbouring Seas of Cheju Island. *Bull. Korean Fish. Soc*., **27**: 515– 528

Kim, J. Y. 1992 The early life history and recruitment of anchovy, Engraulis japonica, in the southern waters of Korea. Ph D thesis, National Fisheries University, Pusan, Korea, p. 238

Kim, W. S., J. –M. Yoo and C. –S. Myung 1993 A review on the copepods in the South Sea of Korea. *Bull. Korean Fish. Soc*., **26**: 266–278

Kirinich, A. R. and D. Hebert 2005 The structure of the coastal density front at the outflow of Long Island Sound during spring 2002. *Continental Shelf Research*, **25**: 1097–1114

Kosro, P. M. 1985 Shipboard acoustic current profiling during the coastal ocean dynamics experiment. Scripps Institution of Oceanography, Ref., 85–8, p. 119

Lee, D. –I. and J. –K. Kim 2007 Numerical Simulation of Residual Currents and Low Salinity Dispersions by Changjiang Discharge in the Yellow Sea and the East China Sea. *Journal of the Korean Society for Marine Environmental Engineering*, **10**: 67–85

Lee, H. –J. and C. Cho 1997 Surface Current Fields in the Eastern East China Sea. *J. Oceanol.Soc. Korea*, **32**: 1–7

Lukens, R. R. and C. Selberg 2004 Guideline for Marine Artificial Reef materials second edition. Artificial Reef Subcommittees of the Atlantic and Gulf States Marine Fisheries Commissions, p. 198

Mack, A. P. and D. Hebert 1999 Mixing structure of high–frequency internal waves in the upper eastern equatorial Pacific. *J. Phys. Oceanogr*., **29**: 3090–3100

Mann, K. H. and J. R. N. Lazier 1991 Dynamics of marine ecosystems. Blackwell, p. 466

Markaki, Z, M. D. Loÿe–Pilot, K. Violaki, L. Benyahya and N. Mihalopoulos 2010 Variability of atmospheric deposition of dissolved nitrogen and phosphorus in the Mediterranean and possible link to the anomalous seawater N/P ratio. *Marine Chemistry*. **120**: 187–194

Miles, J. W. 1961 On the stability of heterogeneous shear flows. *Journal of Fluid Mechanics*, **10**: 496–508

MLTM 2008 Improvement of Fishing Ground Environments using Artificial Upwelling (5th year). Ministry of Land, Transport and Maritime Affairs, Seoul, Korea, p. 429

Mohn, C., J. Bartsch and J. Meincke 2002 Observations of the mass and flow field at Porcupine Bank. *ICES J. Mar. Sci*., **59**: 380–392

Mohn, C. and A. Beckmann 2002 Numerical studies on flow amplification at an isolated shelf break bank, with application to Porcupine Bank. *Continental Shelf Research*, **22**: 1325–1338

MOMAF 2002, 2005a, b, 2006, 2007 Tentative method of oceanic environment process. Ministry of Maritime Affairs and Fisheries, Seoul, Korea

Mullineaux, L. S. and S. Mills 1997 A test of the larval retention hypothesis in seamount generated flows. *Deep–Sea Research*, **44**: 745–770

NFRDI 2005 Gyeongsangnam–do, The artificial reef fishing ground management and observation annual report of 2004, National Fisheries Research and Development Institute, p. 661

Odamaki, M. 1989 Tides and tidal currents in the Tsushima Strait. *J. Oceanogr. Soc. Japan*, **5**: 65–82

OECD 1997 Towards sustainable fisheries: country reports–Korea. OECD Report No. OCDE/GD(97)199, Organization for Economic Co–operation and Development (OECD), Paris, France, pp. 381–391

Owens, W. B. and N. G. Hogg 1980 Oceanic observations of stratified Taylor columns near a buoy. *Deep–Sea Research*, **27**: 1029–1045

Park, C. and J. K. Choi 1997 Zooplankton Community in the Front Zone of the East Sea of Korea (the Sea of Japan) : 1. Species List, Distribution of Dominant Taxa, and Species Association. *Bull. Korean Fish. Soc* ., **30**: 225–238

Pickard, G. L. and W. J. Emery 1990 Descriptive Physical Oceanography. Pergamon Press, p. 320

Pingree, R. D., P. R. Pugh, P. M. Holligan and G. R. Foster 1975 Summer phytoplankton blooms and red tides along tidal fronts in the approaches the English Channel. *Nature*, **258**: 672–677

RD Instruments 1989 Principles of operation: A practical primer, p. 36

Rippeth, T. P., M. R. Palmer J. H. Simpson, N. R. Fisher and J.

Sharples 2005 Thermocline mixing in summer stratified continental shelf seas. *Geophysical Research Letters*, **32**: L05602

Roden, G. I. and B. A. Taft 1982 Effect of Emperor Seamounts on the mesoscale thermohaline structure during the summer of 1982. *J. Geo. Res*., **90**: 839–855

Ryther, J. H. 1969 Photosynthesis and fish production in the sea, The production of organic matter and its conversation to higher forms of life vary throughout the world ocean. *Science*, **166**: 72–76

Seaman, W. Jr. 2000 Artificial reef evaluation: with application to natural marine habitat. CRC Press, Boca Raton, Florida. p. 38

Simpson, J. H., P. B. Tett, M. L. Argote–Espinoza, A. Edwards, K. L. Jones and G. Savidge 1982 Mixing and phytoplankton growth around and island in a stratified sea. *Continental Shelf Research*, **1**: 15–31

Skyllingstad, E. D. and H. W. Wijesekera 2004 Large–eddy simulation of flow over two–dimensional obstacles: high drag states and mixing. *J. Phys. Oceanogr*., **34**: 94–112

Suzuki, T. 2002 Ocean Fertilization by the man–made Sea–Mountains Built with Coal Ash Concrete Blocks. Proceedings of The Twelfth (2002) International Offshore and Polar Engineering Conference, pp. 734–736

Trasviña–Castro, A., G. Gutierrez de Velasco, A. Valle–Levinson, R. González–Armas, A. Muhlia and M. A. 2003 Hydrographic observations of the flow in the vicinity of a shallow seamount top in the Gulf of California. Estuarine, *Coastal and Shelf Science*, **57**: 149–162

van Haren, H., L. Mass, J. T. F. Zimmerman, H. Ridderinkhof and H. Malscharet 1999 Strong inertial currents and marginal internal wave stability in the central North Sea. *Geophysical Research Letters*, **26**: 2993–2999

White, M., C. Mohn and M. Orren 1998 Nutrient distributions across the Porcupine Bank. *ICES J. Mar. Sci*., **55**: 1082–1094

White, M., C. Mohn, H. de Stigter and G. Mottram 2004 Deep–water coral development as a function of hydrodynamics and surface productivity around the submarine banks of the Rockall Trough, NE Atlantic. In: A. Freiwald and M. Roberts (2005), Eds. Deep water corals and ecosystems. Springer–Verlag Berlin Heidelberg, pp. 503–514

Yanagi, T. and M. Nakajima 1991 Change of oceanic condition by the man–made structure for upwelling. *Marine Pollution Bulletin*, **23**: 131–135